Sensors & Transducers, Vol. 204, Issue 9, September 2016, pp. 58-67

Sensors & Transducers

http://www.sensorsportal.com

Fabrication of Micromachined SnO_2 Based MOS Gas Sensor with Inbuilt Microheater for Detection of Methanol

*** Priyanka Kakoty, Manabendra Bhuyan**
Tezpur University, Tezpur, Assam, India
* E-mail: priyankak@tezu.ernet.in

Received: 4 July 2016 /Accepted: 31 August 2016 /Published: 30 September 2016

Abstract: This paper presents a simple method to fabricate a vertical closed membrane structured gas sensor on silicon substrate using micromachining technology for methanol detection at lower concentration. An undoped tin dioxide thin film is deposited by DC magnetron sputtering technique on a pair of gold interdigitated microelectrodes of dimension 820 µm×925 µm. A meander shaped platinum micro heater of dimension 1025 µm×1000 µm is incorporated to provide optimum operating temperature (about 350 ^{0}C) for sensing operation. Energy dispersive X-ray spectroscopy is done to confirm the chemical composition of the sensor. Temperature coefficient of resistance of the inbuilt micro heater is found to be 0.0941 /^{0}C. The sensor resistance shows significant change when micro heater voltage is varied from 1.5 V-3 V. I-V analysis of the sensor is carried out at 25 ^{0}C, 50 ^{0}C and 75 ^{0}C, and shifts in current through the sensor at different temperatures are observed. I-V characterization is also carried out at different methanol concentration levels (50-110 ppm) and it is found that at minimum 80 ppm, the sensor exhibits promising result. The response time and recovery time of the sensor is found to be 160 s and 167 s respectively. *Copyright © 2016 IFSA Publishing, S. L.*

Keywords: Gas Sensor, Methanol sensing, Low concentration, Inbuilt micro heater.

1. Introduction

Methanol is a highly toxic organic solvent and its significant exposure can cause serious effect in human health [1]. However, this solvent has wide applications in the field of manufacturing of drugs, perfumes, dyes, etc. and also in power sources [2]. Therefore, it is necessary to develop a reliable sensor that is capable of detection of methanol at even low concentration levels.

Methanol sensors have been developed based on capacitive sensor using Cu-BTC nanoporous film [3], nanocomposite deposited on PMMA-G-CNT nanocomposites [4], molecularly imprinted techniques [5], SiC-FET [6], magnetic nano emulsion [7], catalyst electrode of Pt dots [8], hydrothermally prepared αFe_2O_3 co doped SnO_2 nanocubes [9], hydrothermally prepared SnO_2/MWCNTs composites [10] etc. Sensors based on metal oxides show excellent performances like high stability, low cost, flexibility in production, high sensitivity, compact size and wide application [11]. Although there are many metal oxides that show good gas sensing properties, SnO_2 have been intensively studied for methanol sensing owing to its various physical characteristics that makes it a popular gas sensing material [12] to various oxidizing and reducing gases. The adsorption/ desorption process of oxygen and the gas molecules at the sensor surface governs the sensing mechanism of SnO_2 towards methanol. At elevated temperature, the atmospheric oxygen is converted to different ionic form such as O_2^-, O^-, O^{2-} by acquiring the trapped electrons from the conduction band which are consequently liberated back when exposed to

methanol as it decomposes following a dehydrogenation path. The chemical reactions were discussed in details in [1] and [13]. It was proposed in [14-17] that at an operating temperature between 300^0C - 350^0C, the sensitivity of pure SnO_2 film is maximized to reducing gases. At this temperature range, the O^- is highly active and acts as the dominating ionic species of oxygen present in the surface of the metal oxide sensing layer which dominates the decomposition reaction of methanol when exposed to the sensing surface layer. Moreover, SnO_2 is a low cost material with high sensitivity which also shows simplicity in fabrication and has been developed for methanol sensing in different forms by different techniques. Various deposition techniques for methanol sensing found in literature are sol-gel or hydrothermal and deposited by either dip-coating [18], spin-coating [19], screen printing [20-22], and electrospinning [23-25] deposition techniques in either Si/glass/ceramic/alumina substrates. SnO_2 for methanol sensing has also been deposited by thermal evaporation technique in [26-27], in which 200 ppm methanol was the lowest concentration as described in [26]. PECVD technique has also been employed by researchers to deposit SnO_2 [28-29] where 30 ppm methanol was used as test concentration. Different nanostructures of SnO_2 have also been developed for methanol sensing e.g. nanorods [28-29], nanofibres [23-25], nanowires [26-27], nanocubes [9], nanoflowers [30] and as nanocomposites [20, 25] with other metal oxides like ZnO, In_2O_3, TiO_3, Fe_2O_3, etc. In case of the doped SnO_2 based methanol sensor, various metals like Pd, Al, Zn, CdS, etc. have also been used [21-22, 31]. Thin films as well as thick films of SnO_2 as methanol sensing material has also been widely embraced by the researchers [18-19, 22] which have shown reasonably good performance in terms of sensitivity, response/recovery time and operating temperature. A good response time of 5 s is achieved in [18] but the sensor responds to methanol concentration greater than 40000 ppm only. In [19-20] also, the reported lowest methanol concentration responded by the sensor is 200 ppm and '1 % of volume' respectively. Many researchers have reported [23-25, 28-29] about the use of SnO_2 in various forms, for sensing methanol in lower concentrations. For example in [23, 25], they have achieved response of the sensor at 10 ppm and in [29] achieved response at 30 ppm concentration. Response for a wide range of concentration level were reported in [24] for 2-600 ppm and in [28] for 10-100 ppm, but in all the cases [23-25, 28-29], operating temperature of about 250-350 ^{0}C was applied externally which requires a separate temperature controlled setup. A lower operating temperature, say at room temperature, was reported in [18]. However, the sensitivity of the sensor to low concentration of methanol is very poor, i.e. >40,000 ppm. In the present work an attempt has been made to develop a novel methanol sensor using undoped SnO_2 as the sensing material for reliable detection of methanol at low concentration with reasonably fast response and recovery time. The sensor is fabricated with an inbuilt micro heater to facilitate selection of optimum operating temperature.

For an efficient metal oxide semiconductor (MOS) gas sensor development, higher sensitivity at low concentration, lower response time and lower operating temperature is desired. In this work, an effort has been made to deposit a thin film SnO_2 based MOS gas sensor using Si micromachining technology for detection of low concentration of methanol at relatively faster response time at optimum operating temperature which also consumes low power.

2. Units of the Gas Sensor Module

The proposed gas sensor mainly comprises of a heater, electrodes and the gas sensitive layer on a thin dielectric membrane deposited on Si substrate. A computer-aided design software, Clewin 4.0, is used to design the masks required in the fabrication process. In this work, five masks (top cavity for sensing element, interdigitated electrodes, isolator, micro heater, and bottom cavity) has been prepared to develop the gas sensor using micromachining technology.

2.1. Interdigitated Electrodes

In this design, gold electrodes are placed beneath the sensing SnO_2 film are used with interdigitated structure as it maximizes electrode sensitivity and minimizes performance variability. The alternating pattern of the electrode fingers creates a densely fit sensing region between the opposing rails by creating greater interaction area between the opposing leads. Fig. 1 shows the mask of interdigitated electrode structure designed for fabrication.

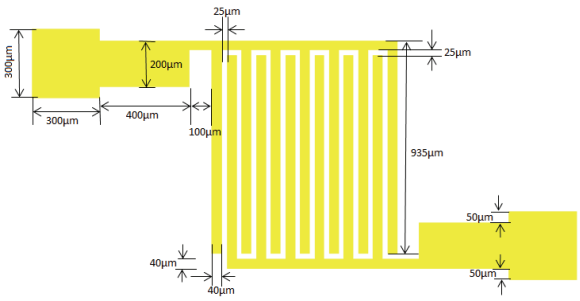

Fig. 1. Interdigitated electrode mask used in the gas sensor.

2.2. Microheater Element

The change in conductivity upon gas exposure of MOS is poor at room temperatures, so micro heater is incorporated to get an optimum working temperature for gas sensing. A platinum micro heater is designed to produce optimum temperature and is deposited over a SiO_2 dielectric membrane. Platinum is selected for

micro heater as it is suitable for high temperature, electrically and thermally stable at high temperature and also highly conductive [32]. The presented micro heater design provides a uniform temperature distribution with low power consumption of 1.33 mW at a lower applied voltage of 2 V. Fig. 2 shows the dimension of the mask of the meander shaped micro heater used in this gas sensor.

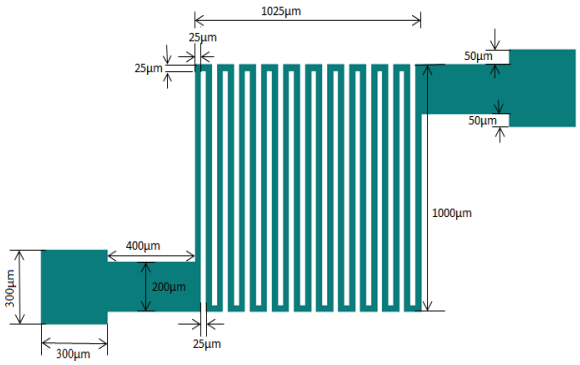

Fig. 2. Meander shaped micro heater mask used in the gas sensor.

2.3. Substrate

Silicon has excellent mechanical properties and the electronics circuits and the sensor can also be assimilated on a single chip. To achieve negligible power loss closed membrane type structure was used. Thermal response of closed membrane type is also better than the other type i.e. suspended membrane type. Hence, in this work, it is adopted by deep reactive ion etching (DRIE) from the backside of the Si substrate so that the active area of the sensor is located only on the thermally isolated dielectric membrane of SiO_2.

2.4. Sensing Layer

The sensing film is the SnO_2 layer which is deposited at the top of the vertical structure, over the fingers of the interdigitated electrodes which remains exposed to the target gas. Sputtering technique is employed in this work for uniform deposition of SnO_2 as the sensing layer.

3. The Fabrication Process

Si micromachining technology is used for the fabrication process as it is one of the most advantageous technologies to manufacture conductometric MOS gas sensors [33-34]. The fabrication process was started with a silicon wafer (4 inch, 450 µm-thick, p-type, and <100> oriented, single sided polished) (Fig. 3 (a)). The wafer is oxidized by thermal oxidation method at 1100^{0}C for 8 hours to obtain 2 µm of SiO_2 both on front and backside of the wafer (Fig. 3 (b)). The front layer is used as the membrane to support the active sensing layer, whereas the back layer is used as an inductively coupled plasma (ICP) etching hard mask. Then photolithography was carried out by coating with AZ5214 (a positive photoresist) by spin coating (*model: Laurell spin coater*) at 4000 rpm for 40 s, followed by a soft bake at 110 ^{0}C for 1 min (Fig. 3 (c)) on the hotplate. Subsequently, the micro heater mask transfer was done in mask aligner (*model: Karl Suss MJB4 double sided mask aligner*) with exposure time of 8 s. The developer used was MF26A for 21 s (Fig. 3 (d)). Ti/Pt micro heater of 10/60 nm was then deposited (Fig. 3 (e)) on the substrate by DC magnetron sputtering system (*model: Techport sputter coater; target to substrate distance: 7.5 cm; deposition: stationary deposition; base pressure: 4.6×10^{-6} Torr; deposition pressure:6.7×10^{-6} Torr; temperature: room temperature; power: 35 W/150 W; gas used: Argon at 250 sccm; pre-sputter time: 1200 s; deposition time: 35/210 s*). Then Platinum (Pt) lift off was done by dipping in acetone and Isopropyl alcohol (IPA) rinse which revealed the required patterned micro heater shown in Fig. 3 (f).

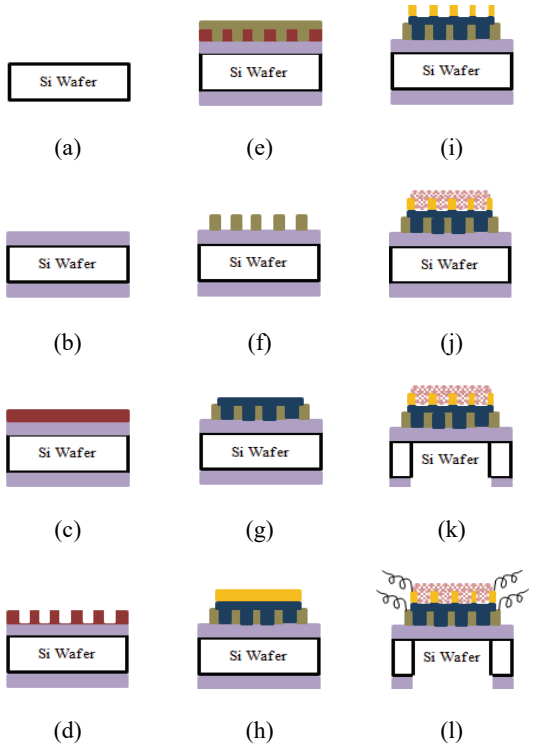

Fig. 3. Fabrication process flow of the gas sensor.

The optical photograph of the micro heater is shown in Fig. 4(a).

Then an insulating layer (SiO_2) of 300 nm (Fig. 3(g)) is deposited over the micro heater so that there is no electrical connection between the micro heater and microelectrodes as well as the metal oxide sensing layer. SiO_2 is a material with low thermal conductivity, provide good thermal isolation to the substrate and is useful in spreading the temperature of the heater uniformly to its upper layers. A blanket film

of SiO_2 was deposited by e-beam evaporation *(model: Techport ebeam evaporator; deposition rate: 1 Å/sec; deposition pressure: 2.5×10^{-6} Torr; deposition temperature: room temperature; no process gases used*) which was patterned by lithography and etched by reactive ion etching (RIE) (*time: 2 min; gas used: CHF3 (40 sccm); chamber pressure: 5 mTorr; He baking pressure: 10 Torr; process temperature: 0^0C; ICP power: 1500 W; RF power: 50 W; etch rate: 180 nm/min*) to remove the layer from the contact pads of the micro heater. The optical microscopic photograph after SiO_2 deposition is shown in Fig. 4(b).

After that, photolithography and mask transfer of the microelectrode was carried out on the wafer and then Cr/Au of 10/60 nm electrode was deposited by DC magnetron sputtering (Fig. 3(h) (*distance of target to substrate: 7.5 cm; deposition: stationary deposition; base pressure: 5×10^{-6} Torr; deposition pressure: 6×10^{-6} Torr; temperature: room temperature; power: 100 W/25 W; gas used: Argon at 50 sccm; pre-sputter time: 600/10 s; deposition time: 22/180 s*), followed by a lift off process to obtain the desired pattern of microelectrodes (Fig. 3(i)). Visual inspection was done and the patterned microelectrodes are observed using microscope and is as shown in Fig. 4(c).

Subsequently, 50 nm SnO_2 sensing layer was deposited on the substrate by DC magnetron sputtering in a Techport sputter system (*target to substrate distance: 9 cm; deposition: stationary deposition; base pressure: 5×10^{-6} Torr; deposition pressure: 6.5×10^{-3} Torr; temperature: room temperature; power: 60W RF source; gas used: Argon at 250 sccm; pre-sputter time: 600 s; deposition time: 40 min*) which was patterned by photolithography and lift off process (Fig. 3(j)). The microscopic image of the sensor is as shown in the Fig. 4 (d).

The wafer was annealed at 500 ^{0}C for 1hr and then coated with AZ4562 (a positive photoresist) both on front and backside by spin coating (*at 4000 rpm for 40 s*). A soft bake was followed at 110 ^{0}C for 90 s in the hotplate. The mask pattern of the fifth mask (1.7 mm×1.7 mm) for backside etch was then transferred to the photoresist using UV light (*model: EVG 620 double sided mask aligner; contact: proximity contact; dosage: 110 mJ/cm^2*) and developed using MF26A for 25 s, then hard bake was done at 110^{0}C for 3 min.

Consequently, RIE was carried out backside to etch the 2 µm SiO_2 on the wafer (*model: Oxford instruments plasma technology; ICP-RIEF; etching time: 12 min; etch rate: 200 nm/min; ICP power: 1500 W; Rf power: 50 W; chamber pressure: 5 mTorr; gases used: CHF3 (40 sccm); process temperature: 0 ^{0}C; helium pressure: 10 Torr*). The wafer was then processed by DRIE on backside for etching Si (*etching time: 13 min; etch rate: 30 µm/min; etch cycle pressure: 220 mTorr; gases used: C4F8 (250 sccm) and SF6 (600 to 450 sccm); process temperature: -10 ^{0}C in Hf generator mode; ICP power: 4500 W; Rf power: 80 W*). After that the wafer was cleaned with IPA and acetone to strip the photoresist and dried with N_2 drier (Fig. 3 (k)).

The closed membrane structure was confirmed by measuring the cavity height with a profiler (*model: Dektak XT stylus profiler*). After completion of sensor fabrication, wire bonding was done to perform electrical characterization (Fig. 3 (l)).

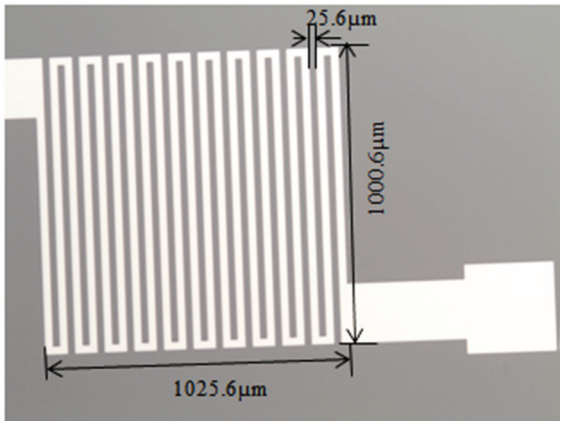

Fig. 4 (a). Microscopic image of Pt micro heater.

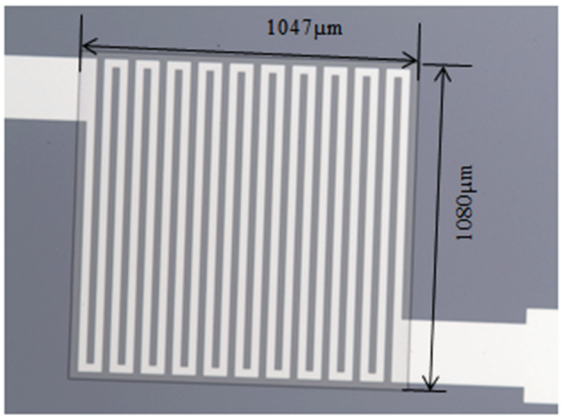

Fig. 4 (b). Microscopic image of SiO_2 insulating layer over the micro heater.

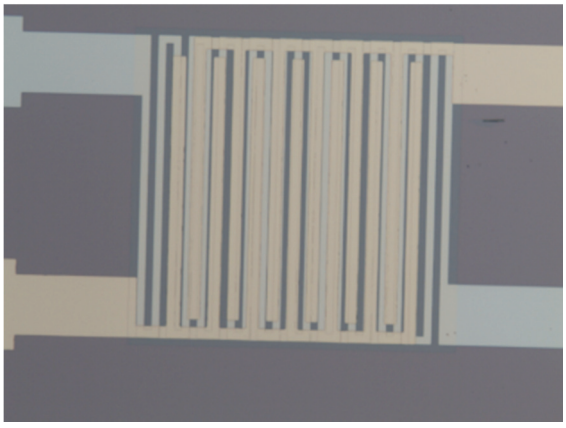

Fig. 4 (c). Microscopic image of Au electrodes over SiO_2 layer.

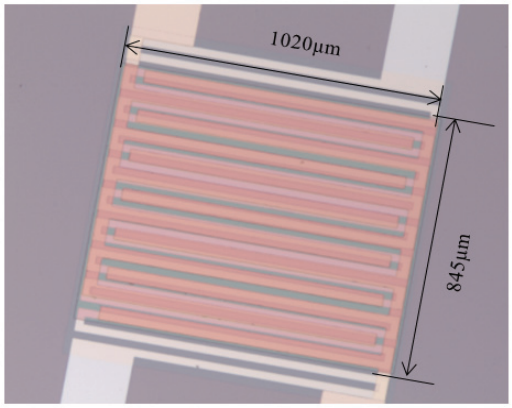

Fig. 4(d). Microscopic image of after deposition of SnO_2 layer.

(Resolution of the microscope=1 μm; Magnification=5x).

4. Structural Characterization

4.1. XRD and EDS Analysis

Structural analysis of SnO_2 target used for sputtering the sensing material was carried out using an X-ray Diffractometer (*Bruker AXS, D8 focus*) with CuKα radiation as an X-ray source at 40 kV and 30 mA in the scanning angle (2θ) from 10^0 to 70^0 with a scan speed of 0.02^0/s. The diffraction peaks, as shown in Fig. 5, can be indexed to standard pure bulk SnO_2 with a tetragonal rutile structure (JCPDS card No. 041-1445) [35-36].

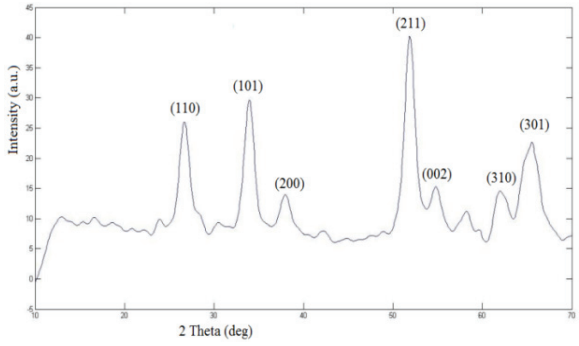

Fig. 5. XRD patterns of sputtered SnO_2 sensing material.

The SnO_2 sensing element shows reflections corresponding to major characteristic peaks at (110), (101), (200), (211), (002), (310) and (301). The average crystallite size (D) of SnO_2 target material was calculated to be 12.18 nm using the first diffraction peak <110> by Debye-Sherrer formula [37]:

$$D = \frac{0.9\lambda}{\beta Cos\theta},$$

where λ is the wavelength of the incident X-ray (1.54Å), β is the full width at half maximum intensity of the distinctive peak (0.7 degree), and θ is the Bragg's angle. Fig. 6 shows the EDS spectra which also confirm the chemical composition of the gas sensor with O, Si, Sn, Au and Pt in it. The presence of Sn and O is due to the SnO_2 layer. The peaks representing Si, Pt, and Au are due to Si substrate, Pt micro heater, Au electrodes. Presence of SiO_2 layer also contributes in increase in wt% of the element O. O content is somewhat higher also due to O_2^- (ads) present in the sample. The sensor photograph after completion of the device is shown in Fig. 7.

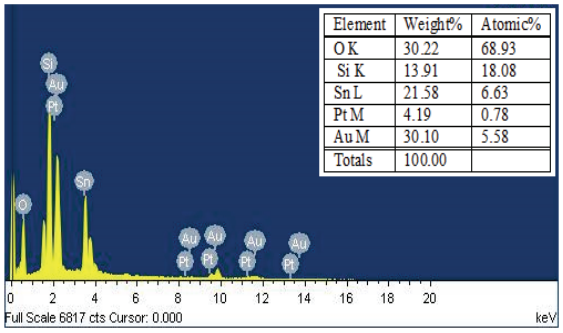

Fig. 6. EDS spectra of the fabricated gas sensor.

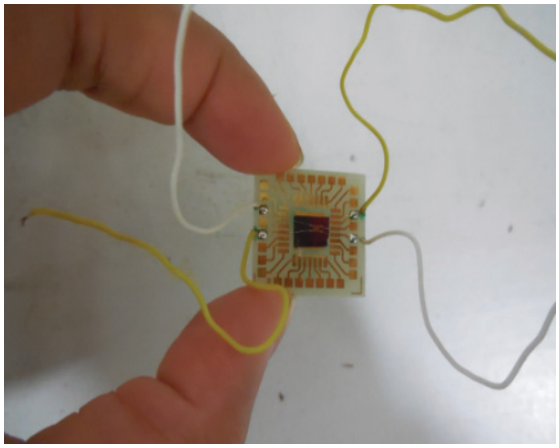

Fig. 7. Photograph of the complete device.

5. Electrical Characterization

5.1. The Microheater

Temperature dependent I-V measurements of the micro heater were carried out in dc probe station (*model: PM5 with thermal chuck, Agilent Device Analyzer B1500A*) and the response found is shown in Fig. 8.

The resistance of the micro heater can be expressed as a function of temperature by the following Equation:

$$R = R_0[1 + \alpha(T - T_0)] \quad (1)$$

or

$$\alpha = \frac{\frac{R}{R_0} - 1}{T - T_0},$$

where R_0 is the resistance measured at ambient temperature T_0=25 ^{0}C, R is the resistance at a temperature T and α is the temperature coefficient of resistance.

From the I-V characteristics of Fig. 8, the values of resistances at different temperatures are found as – $R_0 = R_{25^oC}$ = 1242.274 Ω, R_{50^oC} = 1271.669 Ω, R_{100^oC} = 1331.831 Ω, R_{150^oC} = 1387.93 Ω and R_{200^oC} = 1442.101 Ω.

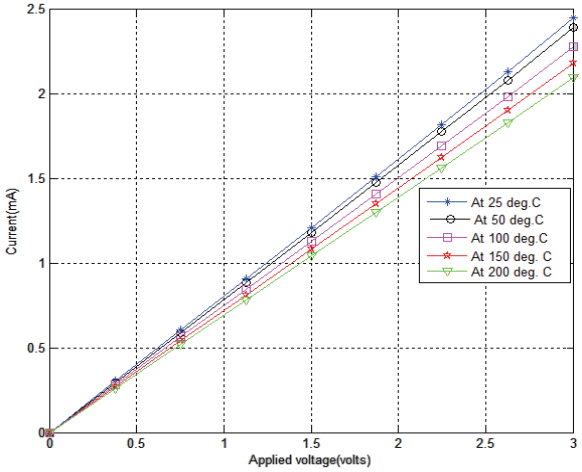

Fig. 8. I-V characteristics of the micro heater at room temperature.

Using the above relation, values of α was calculated at different temperatures (50 ^{0}C to 200 ^{0}C) as shows in Table 1:

Table 1. α at different temperatures.

Temperature (^{0}C)	α (/^{0}C)	α (average) (/^{0}C)
50	0.0946	0.0941
100	0.0961	
150	0.0938	
200	0.0919	

Using the average value of α, the variation in resistance with temperature is obtained and shown in Fig. 9, which shows that the resistance of the micro heater varies linearly with applied temperature. Fig. 10 shows the variation of temperature of the micro heater with applied voltage from which the appropriate voltage to be applied to get the required temperature is obtained.

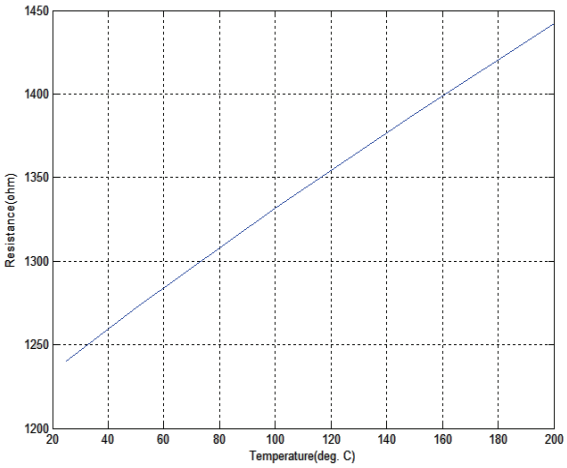

Fig. 9. Resistance change as a function of temperature for the platinum micro heater.

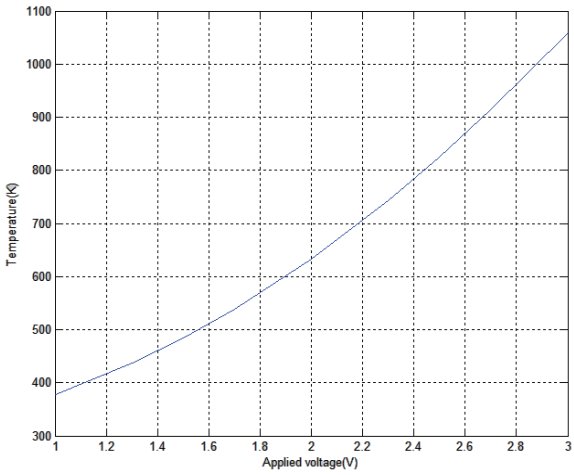

Fig. 10. Variation of temperature with applied voltage of the micro heater.

5.2 The Sensor

5.2.1. Effect of Variation of Heater Voltage on Sensor Resistance

Fig. 11 shows the sensor resistance variation with heater voltage without gas exposure. The response indicates that up to 1.5 V, there is not much change in sensor resistance, but beyond that the sensor resistance significantly increases. Therefore 2 V was chosen as the safe heater voltage to obtain gas response which generates a temperature of about 350 ^{0}C which is sufficient for methanol sensing by the fabricated SnO_2 gas sensor.

5.2.2. Gas Sensing Measurement

The fabricated sensor was connected in a circuit (Fig. 12), where R_H, R_S and R_L are the heater resistance, sensor resistance and load resistance respectively, while, V_H, V_S and V_O represent the heater

voltage, sensor voltage and voltage across the load resistance respectively. The gas sensing and data acquisition set up (schematic is shown in Fig. 13), consists of a sample chamber of 180 ml, three digitally controlled pumps (P1, P2, P3), a sensor chamber with effective volume of 250 ml, power supplies, relays to control the pumps for gas and air flow into and out of the sensor chamber. The total volume of the measurement set-up is the combined volume of the gas chamber, pipes and the sensor chamber which is of 446.328 ml.

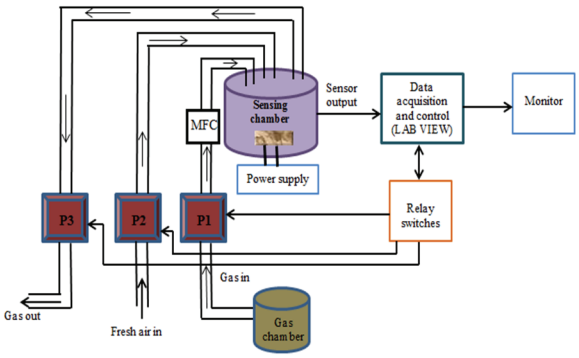

Fig. 13. Schematic of gas sensing measurement system set-up.

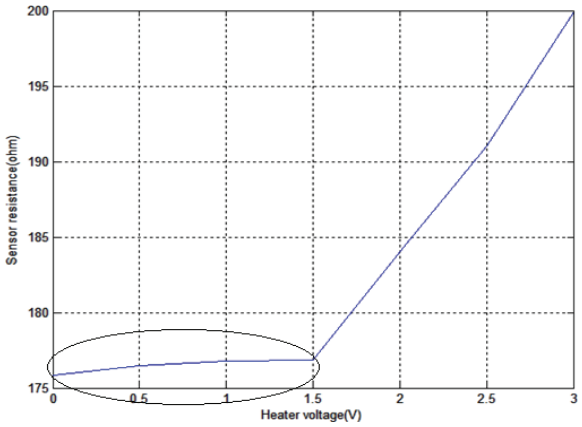

Fig. 11. Variation of sensor resistance with heater voltage.

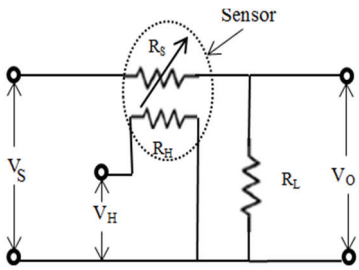

Fig. 12. Electrical circuit used for measuring gas response.

The data acquisition and gas/air flow control was accomplished by a 12-bit data acquisition card (PCI-6024E) with Lab VIEW software from National Instruments which is also used to record and monitor the sensor response. The injected liquid methanol (32.04 g/mol, 99 % purity from Sigma-Aldrich chemical) after vaporization in the gas sample chamber is drawn into the sensor chamber by pump P1. The gas flow rate to the sensor chamber was controlled at 0.8 slpm using a mass flow controller (MFC) (*model: Alicat MC-05slpm-D*). Any change in V_O signifies a change in sensor resistance. The experiment was carried out at room temperature (25 ^{0}C). V_S was kept at 5 V throughout the experiment. The response towards methanol was then tested for five different micro heater voltages (V_H) starting from 0.5 V to 2.5 V with an increase in steps of 0.5 V. The sensor responses for methanol with these micro heater voltages are as shown in Fig. 14. It is seen that the sensor response to methanol with V_H less than 0.5 V is very low. Although at 0.5 V or 1.0 V it shows a feeble response, but the sensor shows a reasonably good response on application of 2 V at the heater terminals.

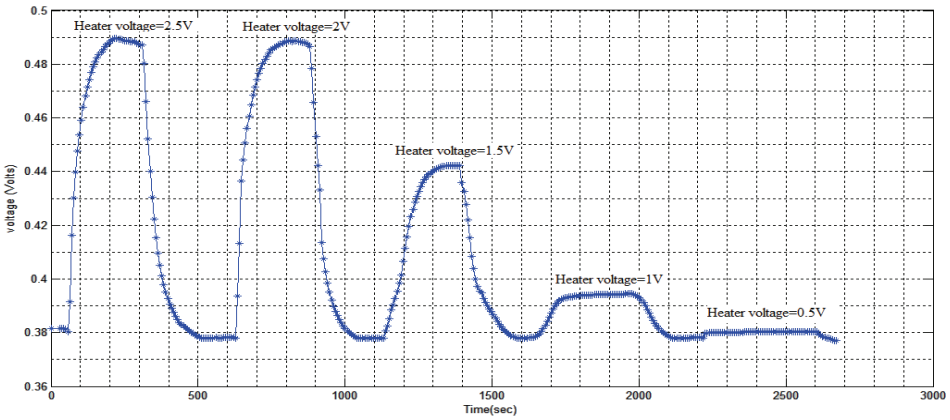

Fig. 14. Gas sensor response at 80ppm methanol with varying heater voltages.

When this voltage is further increased up to 2.5 V, it is observed that the response remains similar to that of the response when 2 V is applied. The sensor response was not tested for any other higher voltage as more heating may cause damage to the active area of the sensor. Moreover, it has also been stated in literature that in a much higher operating temperature range, the desorption of surface-adsorbed oxygen ions

dominates which reduces the sensing film resistance and the gas sensitivity [21]. From the best response it is found that the response reaches a stable value after 160 s which is maintained up to 250 s. After 250 s, the sensor chamber is refreshed with fresh air by operating pumps P2 and P3 for 360 s and it took 167 s to refresh the sensor back to its baseline value. The response, being a first order response, the rising time constant as calculated at 63.2 % of the saturated value and is found to be 42.5 s and the falling time constant was found to be 41.2 s at 36.8 % of the saturated value.

5.2.3. I-V Characterization

For analyzing the temperature effect on I-V characteristic, this characterization was performed at three different temperatures 25 ^{0}C (room temperature), 50 ^{0}C and 75 ^{0}C by changing the sensor bias voltage from -5 V to +5 V DC (Fig. 15). The I-V curve tends to shift to a higher value with rise in temperature and exhibits ohmic behavior.

The I-V characteristics were also studied with different ppm levels of methanol with varying sensor bias voltages. To do so, liquid methanol of different volumes was micropippeted into a sample chamber and the concentration was calculated using the Equation (2) [38] -

$$C = \frac{V_{liq} \times d_{liq} \times R \times T}{V_{total} \times M \times P} \times 10^3, \qquad (2)$$

where C is the desired gas phase concentration in ppm, V_{liq} is the liquid methanol injected by micropipetting (µl), d_{liq} is the density of methanol (0.79 gml^{-1}), V_{total} is the total volume in ml, M is the molecular weight (32.04 gmol^{-1}), P is pressure in the laboratory (0.992 atm), R is the ideal gas constant (0.08206 Latmmol^{-1}K^{-1}), T is the laboratory temperature (298 K).

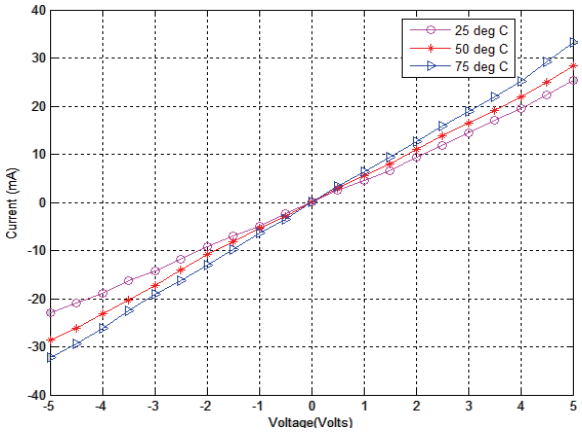

Fig. 15. I-V characteristic of the sensor at different temperatures without gas exposure.

Table 2 shows the different concentration levels used in the experiment. It was observed that the minimum ppm level to which the sensor shows a reasonable response is 80 ppm. In Fig. 16, a rise in current values was detected with increase in concentration of methanol levels, and it is observed that the sensor undergoes a significant change at 80 ppm. On application of concentrations higher than 80 ppm, it was found that there is only a small rise in current.

Table 2. The concentration levels of methanol obtained by micropipetting.

V_{total}	V_{liq} (µl)	Concentration (ppm)
446.328 ml	36.71	50
	44.05	60
	51.4	70
	58.75	80
	66.08	90
	73.43	100
	80.77	110

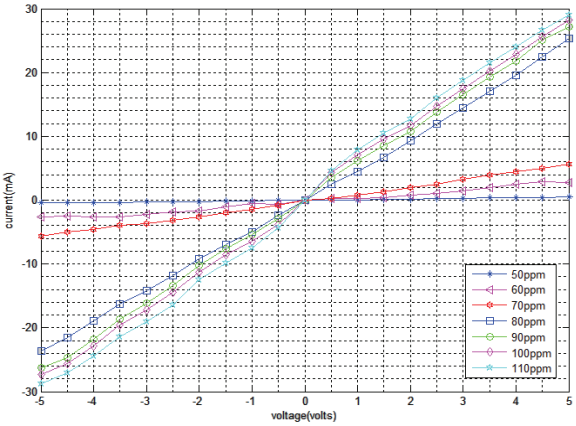

Fig. 16. I-V characteristics with varying methanol concentration (V_H=2 V).

6. Conclusions

An effort has been made in this work to design, fabricate and characterize an undoped thin film SnO_2 based MOS gas sensor for detection of methanol. This vertical structured gas sensor is incorporated with an inbuilt meander shaped platinum micro heater and a pair of interdigitated gold microelectrodes. The micro heater is used to provide the optimum operating temperature to the sensing film while the microelectrodes is used to sense the change in resistance of the sensing film on exposure to gas molecules. XRD, EDS and microscopic imaging is done as a part of structural characterization. For electrical characterization, several experiments like I-V analysis of the micro heater, resistance vs temperature and temperature vs applied voltage analysis of the micro heater were done. The sensor was experimented with micro heater voltage vs sensor

resistance, I-V characterization at different temperatures. I-V characterization of the sensor was also carried out at different concentrations of methanol and it was found that at 80 ppm, the sensor showed reasonable response. The sensor response was also analyzed with different voltages at the micro heater terminals to see its effect on gas sensing. The results obtained is attributed to the processing for the device realization as micromachined gas sensor has the advantages of microsize, identical production of structures all over the silicon wafer, highly uniform, and low power consumption. Significant achievement has been made in this work by depositing SnO_2 thin film for detection of low concentration of methanol, at reasonably fast response and eliminating the need for doping the sensing material.

Acknowledgements

The authors are very thankful to INUP, IISc Bangalore for providing the fabrication facility.

References

[1]. Amit Gupta, J. K. Srivastava, Anand A. Bhaskar, Pd-doped SnO_2 based Thick Film Gas Sensor for detection of Methanol, *International Journal of Innovative Research in Engineering & Science*, Vol. 5, Issue 3, May 2014.

[2]. P. Siciliano, Preparation, characterization and applications of thin films for Gas Sensor s prepared by cheap chemical method, *Sensors and Actuators B: Chemical*, Vol. 70, Issue 1-3, 2000, pp. 153-164.

[3]. M. S. Hosseini, S. Zeinali, M. H. Sheikhi, Fabrication of capacitive sensor based on Cu-BTC (MOF-199) nanoporous film for detection of ethanol and methanol vapors, *Sensors and Actuators B: Chemical*, Vol. 230, July 2016, pp. 9-16.

[4]. Mohammed M. Rahman, *et al*., Sensitive methanol sensor based on PMMA-G-CNTs nanocomposites deposited onto glassy carbon electrodes, *Talanta*, Vol. 150, 2016, pp. 71-80.

[5]. Zhu Q., *et al*., A new and high response Gas Sensor for methanol using molecularly imprinted technique, *Sensors and Actuators B: Chemical*, Vol. 207, 2015, pp. 398-403.

[6]. Darmastuti Zhafira, *et al.,* SiC-FET methanol sensors for process control and leakage detection, *Sensors and Actuators B: Chemical*, Vol. 187, 2013, pp. 553-562.

[7]. Mahendran V., John Philip, A methanol sensor based on stimulus-responsive magnetic nanoemulsions, *Sensors and Actuators B: Chemical*, Vol. 185, 2013, pp. 488-495.

[8]. Yang Jin Seok, *et al*., I–V characteristics of a methanol concentration sensor for direct methanol fuel cell (DMFC) by using catalyst electrode of Pt dots, *Current Applied Physics*, Vol. 10, No. 2, 2010, pp. 370-372.

[9]. Mohammed M. Rahman, *et al*., Fabrication of a methanol chemical sensor based on hydrothermally prepared α-Fe_2O_3 codoped SnO_2 nanocubes, *Talanta*, Vol. 95, 2012, pp. 18-24.

[10]. Aroutiounian V. M., *et al*., Study of the surface-ruthenated SnO_2/MWCNTs nanocomposite thick-film Gas Sensors, *Sensors and Actuators B: Chemical*, Vol. 177, 2013, pp. 308-315.

[11]. Yu-Feng Sun, Shao-Bo Liu, Fan-Li Meng, Jin-Yun Liu, Zhen Jin, Ling-Tao Kong, Jin-Huai Liu, Metal Oxide Nanostructures and Their Gas Sensing Properties: A Review, *Sensors,* Vol. 12, No. 3, 2012, pp. 2610-2631.

[12]. P. Kakoty, M. Bhuyan, SnO_2 based Gas Sensors: Why it is so popular?, in *Proceedings of the IEEE International Conference on Electrical, Computer and Communication Technologies (ICECCT'15),* 2015, pp. 1-5.

[13]. J. Gonzalez-Chavarri, C. Hurtado, G. G. Mandayo, E. Castano, Design and fabrication of sensor structures for the measurement of toxic gases, in *Proceedings of the Spanish Conference on Electron Devices (CDE)*, 2013, pp. 107-110.

[14]. Jayaraman V., *et al*., A low temperature H_2 sensor based on intermediate hydroxy tin oxide, *Sensors and Actuators B: Chemical*, Vol. 55, Issue 2, 1999, pp. 147-153.

[15]. Zhang Gong, Meilin Liu, Effect of particle size and dopant on properties of SnO_2-based Gas Sensors, *Sensors and Actuators B: Chemical*, Vol. 69, 2000, pp. 144-152.

[16]. Cabot A., Arbiol J., Morante J. R., Weimar U., Barsan N., Göpel W., Analysis of the noble metal catalytic additives introduced by impregnation of as obtained SnO_2 sol–gel nanocrystals for Gas Sensors, *Sensors and Actuators B: Chemical*, Vol. 70, Issue 1-3, 2000, pp. 87-100.

[17]. Park Sung-Soon, J. D. Mackenzie, Thickness and microstructure effects on alcohol sensing of tin oxide thin films, *Thin Solid Films*, Vol. 274, No. 1-2, 1996, pp. 154-159.

[18]. Wang H. C., Y. Li, M. J. Yang, Fast response thin film SnO_2 Gas Sensors operating at room temperature, *Sensors and Actuators B: Chemical*, Vol. 119, Issue 2, 2006, pp. 380-383.

[19]. Teeramongkonrasmee A., M. Sriyudthsak, Methanol and ammonia sensing characteristics of sol–gel derived thin film Gas Sensor, *Sensors and Actuators B: Chemical*, Vol. 66, Issue 1-3, 2000, pp. 256-259.

[20]. Wen Zeng, Liu Tian-Mo, Gas-sensing properties of SnO_2–TiO_2-based sensor for volatile organic compound gas and its sensing mechanism, *Physica B: Condensed Matter*, Vol. 405, No. 5, 2010, pp. 1345-1348.

[21]. Cheong H., M. Lee, Sensing characteristics and surface reaction mechanism of alcohol sensors based on doped SnO_2, *Journal of Ceramic Processing Research*, Vol. 7, No. 3, 2006, pp. 183-191.

[22]. Yadava Lallan, Ritesh Verma, R. Dwivedi, Sensing properties of CdS-doped tin oxide thick film Gas Sensor, *Sensors and Actuators B: Chemical*, Vol. 144, Issue 1, 2010, pp. 37-42.

[23]. Tang Wei, Jing Wang, Methanol sensing micro-gas Sensors of SnO_2–ZnO nanofibers on Si/SiO_2/Ti/Pt substrate via stepwise-heating electrospinning, *Journal of Materials Science*, Vol. 50, Issue 12, 2015, pp. 4209-4220.

[24]. Zheng Wei, *et al*., A rapidly responding sensor for methanol based on electrospun In_2O_3–SnO_2 nanofibers, *Journal of the American Ceramic Society*, Vol. 93, Issue 1, 2010, pp. 15-17.

[25]. Tang Wei, *et al*., Hollow hierarchical SnO_2-ZnO composite nanofibers with heterostructure based on

electrospinning method for detecting methanol, *Sensors and Actuators B: Chemical*, Vol. 192, 2014, pp. 543-549.
[26]. Johari Anima, M. C. Bhatnagar, Vikas Rana, Low temperature tin oxide (SnO_2) nanowire Gas Sensor, in *Proceedings of the 16th International Workshop on Physics of Semiconductor Devices. International Society for Optics and Photonics*, 2012.
[27]. Kumar R. Rakesh, *et al*., Novel low-temperature growth of SnO_2 nanowires and their gas-sensing properties, *Scripta Materialia*, Vol. 68, No. 6, 2013, pp. 408-411.
[28]. Forleo Angiola, *et al*., Fabrication at wafer level of miniaturized Gas Sensors based on SnO_2 nanorods deposited by PECVD and gas sensing characteristics, *Sensors and Actuators B: Chemical*, Vol. 154, Issue 2, 2011, pp. 283-287.
[29]. Forleo A., *et al*., Wafer-level fabrication and gas sensing properties of miniaturized Gas Sensors based on inductively coupled plasma deposited tin oxide nanorods, *Procedia Chemistry*, Vol. 1, Issue 1, 2009, pp. 196-199.
[30]. Huang Jiarui, *et al*., Preparation of porous flower-shaped SnO_2 nanostructures and their gas-sensing property, *Sensors and Actuators B: Chemical*, Vol. 147, Issue 2, 2010, pp. 467-474.
[31]. Guan Yue, *et al*., Hydrothermal preparation and gas sensing properties of Zn-doped SnO_2 hierarchical architectures, *Sensors and Actuators B: Chemical*, Vol. 191, 2014, pp. 45-52.
[32]. Bansal Vineet, *et al*., 3-D Design, Electro-Thermal Simulation and Geometrical Optimization of spiral Platinum Micro-heaters for Low Power Gas sensing applications using COMSOL™, in *Proceedings of the COMSOL Conference,* Bangalore, 2001.
[33]. Bochenkov V. E., G. B. Sergeev, Sensitivity, selectivity, and stability of gas-sensitive metal-oxide nanostructures, *Metal Oxide Nanostructures and Their Applications*, Vol. 3, 2010, pp. 31-52.
[34]. V. E. Bochenkov, G. B. Sergeev, Preparation and chemiresistive properties of nanostructured materials, *Advances in Colloid and Interface Science*, Vol. 116, No. 1-3, 2005, pp. 245-254.
[35]. M. Aziz, S. Abbas, W. Baharom, Size-controlled synthesis of SnO_2 nanoparticles by sol-gel method, *Mater. Lett.*, Vol. 91, 2013, pp. 31-34.
[36]. Y. Li, W. Yin, R. Deng, R. Chen, J. Chen, *et al*., Realizing a SnO_2-based ultraviolet light-emitting diode via breaking the dipole-forbidden rule, NPG Asia Mater., Vol. 4, No. 11, 2012, pp. e30.
[37]. I. H. Kadhim, H. A. Hassan, Effects of glycerin volume ratios and annealing temperature on the characteristics of nanocrystalline tin dioxide thin films, *Journal of Materials Science Materials in Electronics*, Vol. 26, No. 6, 2015, pp. 3417-3426.
[38]. Uyanik A., N. Tinkilic, Preparing Accurate Standard Gas Mixtures of Volatile Substances at Low Concentration Levels, *The Chemical Educator,* Vol. 4, Issue 4, 1999, pp. 141-143.